Postharvest Biology and Technology 192 (2022) 112013

Contents lists available at ScienceDirect

Postharvest Biology and Technology

journal homepage: www.elsevier.com/locate/postharvbio

Complementary deep learning and chemometrics: A case of pear fruit centroid detection and spectral model application for fruit spectral image processing

Junli Xu[a], Puneet Mishra[b,*]

[a] School of Biosystems and Food Engineering, University College of Dublin (UCD), Belfield, Dublin 4, Ireland

[b] Wageningen Food and Biobased Research, Bornse Weilanden 9, P.O. Box 17, 6700AA, Wageningen, the Netherlands

ARTICLE INFO

Keywords:
Computer vision
Artificial intelligence
Spectroscopy
Object detection

ABSTRACT

A novel case of combining deep learning and chemometrics for spectral image processing is presented. The case involved the application of deep transfer learning for detecting and locating the fruit centroid to extract pixels for spectral model development and application. The selected fruit case involved a non-symmetrical fruit pear where the interesting area for spectral model application is not the centroid of the whole fruit unlike fruit such as apples but the centroid of the belly part of the pear fruit. Hence, the task of object detection is replaced with the task of symmetrical region (fruit belly) detection on the pear fruit such that the spectral model can be applied in the centroid pixels of the symmetrical region. For spectral modelling, the latent variables based regression technique called partial least-square (PLS) regression was used. For spectral modelling, PLS was preferred over deep learning as there was a low number of samples points to train a deep spectral model. The deep transfer learning allowed 100 % correct detection of the pear fruit belly part with the intersection over union score of 0.82. Furthermore, the RMSEP = 0.77 % was attained with the PLS modelling to predict dry matter. The presented approach can support the wide application of spectral imaging for fresh fruit analysis, particularly when imaging is performed simultaneously on multiple objects and the objects are non-symmetrical in shape.

1. Introduction

Spectral imaging of fresh fruit in the visible and short-wave near-infra-red range (400–1000 nm) of the electromagnetic spectrum is widely performed for the prediction of key quality traits such as dry matter (DM) and soluble solids content (SSC) (Lu et al., 2020). The spectral imaging in 400–1000 nm instead of > 1000 nm is preferred for many reasons. For example, it captures both the colour and 3rd overtones of chemical bond overtones (OH, CH, NH) for macro chemical components in fruit such as water, protein and sugars (Mishra et al., 2020; Walsh et al., 2020), the light penetration depths for the short-wave near-infrared region (700–1000 nm) is higher than the short wave infrared (>1000 nm) (Lammertyn et al., 2000), thus bringing more information from the fruit flesh below the peel. Also, cost-wise, the visible and short-wave near-infrared spectral sensors are up to three times lower in cost as they use the silicon-based detector compared to the InGaAs based detector used by short wave infrared spectral sensors (Mahlein et al., 2018).

For fruit analysis, spectral imaging has the main advantage of being high-throughput compared to the point-based spectral sensing of fruit where the user needs to scan each fruit (Lu et al., 2020). The main advantage of spectral imaging over point-based spectroscopy is the simultaneous procurement of spatial and spectral information from the fruit, allowing the provision of the spatial distribution of physico-chemical parameters, which enhances the perception of quality changes within the fruit (Lin et al., 2021; Rungpichayapichet et al., 2017). For instance, spectral imaging has been applied to visualize the spatial distribution of firmness, total soluble solids and titratable acidity within the mango, which demonstrated that fruit ripening started from the shoulder toward to tip part (Rungpichayapichet et al., 2017). However, the spectral imaging in terms of fresh fruit analysis is still far from routine usage compared to the point-based sensing approaches. For example, the point spectral sensing (Anderson et al., 2020; Subedi and Walsh, 2020) for fresh fruit analysis is now readily available in market with pre-calibrated fruit models. The spectral cameras are still available as sensors that often requires the user to build their own systems and in

* Corresponding author.
E-mail address: puneet.mishra@wur.nl (P. Mishra).

https://doi.org/10.1016/j.postharvbio.2022.112013
Received 15 March 2022; Received in revised form 11 June 2022; Accepted 11 June 2022
Available online 16 June 2022

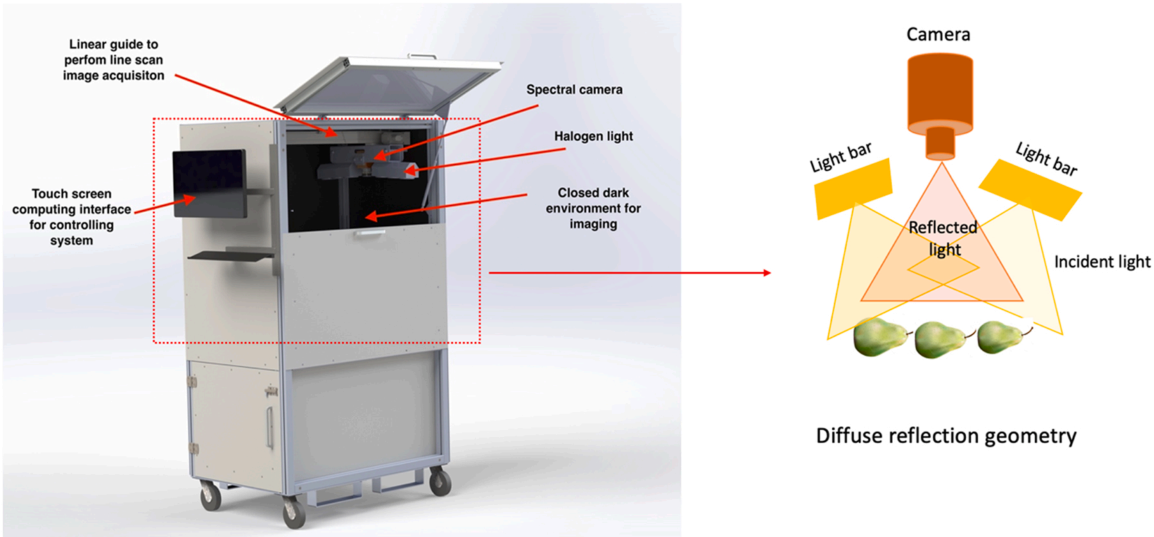

Fig. 1. The All-In-One spectral imaging (Mishra et al., 2022b) system used for spectral image acquisition (Xu and Mishra, 2022).

most cases also requires the development of calibration models for fruit property prediction from scratch (Mishra et al., 2022b).

Recently, a new approach to fully standardised imaging of fresh fruit called all-in-one spectral imaging (ASI) was proposed (Mishra et al., 2022b; Mishra, 2021). The ASI approach to spectral imaging involves integration of all necessary hardware (camera, translation stage, computing system, white reference) and software (acquisition and model deployment) components to control the spectral imaging as well as simultaneous deployment of spectral models for fresh fruit properties prediction. In the ASI framework, the acquisition of images is uniform and standardised for all kinds of fruits. One of the main challenge with the spectral imaging is that it requires controlled illumination (no interference from external illumination) which is achieved with the close cabinet form of the spectral system presented in the recent study (Mishra et al., 2022b). In the ASI framework to spectral imaging, the predictive models can directly be integrated to the computing software such that the data and models can be reused in future applications.

In spectral imaging modelling of fresh fruit for practical application, there are two main steps involved. The first step is the detection of the object while the second step is predicting the chemical properties such as DM in the case of fresh fruit using chemometric analysis. The second step of chemometric analysis depends on object detection as only after object detection the relevant spectra can be extracted for chemometric model development or application. For fresh fruit, the chemometric analysis using the centroid pixels or the region around is desired. This is because most fruits have a curvy shape and the centroid part of a lying fruit is the one that can be considered the most flat, thus, having minimal angular reflections. Such centroid pixels can usually be obtained as the centroid of the detected object marked by the bounding box. However, there are some inherent challenges in the detection of fruit, for example, many times in non-laboratory imaging conditions fruit are touching each other and traditional approaches for fruit detection such as using vegetation indexes combined with threshold are not desirable (Xu and Mishra, 2022). Recently, deep learning was proposed as a solution to perfom object detection in the spectral images (Xu and Mishra, 2022). The approach involved using the already pre-trained object detection models (YOLOv4) and fine-tuning it using some spectral images to detect fruit in the spectral imaged scene. However, such an approach to object detection works when fresh fruit are symmetrical in nature, for example, apples, round berries, grapes as the centroid of the bounding box is the centroid of the fruit which can be used for chemometric analysis. For asymmetrical fruit such as pear, in spite of correctly detecting and localizing the entire fruit using the bounding box, such an approach can only provide the centroid of the bounding box enclosing the complete fruit, which is not representative of the centroid of the region of interest. In such a case, the object detector requires to be modified and updated in order to detect/identify the useful region of interest of fruit of whom centroid matches with the centroid of the bounding boxes. In the case of pear, the key idea is to train the object detector for detecting the belly of the pear fruit. The detection of the belly part of the pear is of great importance and interest because the belly area is often used (by a fruit analyst) for explaining the DM and SSC in pear fruit (Mishra et al., 2021b). Although previous work has demonstrated that the YOLOv4 object detector allows the detection of the whole pear, the potential to identify and localize only the belly part remains unknown, which deserves further investigation since it is practical and relevant in the real application scenario.

The objective of this study was to use deep transfer learning for detecting representable parts on non-symmetrical pear fruit which can later be used for the application of the chemometric models to predict the fruit property. For spectral modelling, latent variables based regression technique called partial least-squares regression was used.

2. Materials and methods

2.1. Dataset

The data set can be understood as having two parts i.e., data for deep transfer learning based object detection and the data for predictive spectral modelling. For DTS, the data consisted of 117 spectral images captured using the ASI setup. The 117 spectral images of 'Conference' pear fruit (*Pyrus communis L.*), origin The Netherlands, were collected in diverse experiments (the year 2020–2021) in the Food & Biobased Research, The Netherlands. The spectral images in the ASI setup were acquired in the spectral range of 398–1000 nm with a spectral spectra interval of ~3 nm with a visible and short-wave near-infrared spectral camera (Fx10, Specim, Oulu, Finland) (Fig. 1). The default exposure time of the camera was 20 ms and the data were recorded in spectral binnin of 2. The speed of the translation stage was set to 30 mm/s. The illumination in ASI was provided using six halogen lights (25 W each) (supplied by Specim, Oulu, Finland) (Fig. 1). The ASI setup is fully automated for acquisition controls such as the speed of the translation stage, exposure time, number of frames, etc. For white reference, the ASI setup has an inbuilt white reference (Teflon). For dark reference, the spectral camera uses automatic shutter closure prior to image acquisition. The captured images were also automatically radiometrically

Table 1
YOLOv4 model performance for detecting pear belly after transfer learning.

Training (Number of objects)	Test (Number of objects)	Average precision	Mean intersection over union score
1818	72	1.00	0.82

corrected using the white and the dark references to provide reflectance data. Note that in this study to perform the deep transfer learning, a subset RGB data set was generated by sampling the spectra bands 671, 534, and 430 nm. The deep transfer learning was performed on RGB images using the pre-trained YOLOv4 model which is trained using the RGB images available in the computer vision domain.

For spectral modelling, 18 spectral images were used as for the fruit imaged (total 216) in those images, reference DM was also estimated. The DM was estimated by sampling a circular disc from the centroid of the fruit belly as described in earlier studies (Mishra et al., 2021b). The circular disk was weighted (XS10001 L, Mettler-Toledo GmbH, Giessen, Germany) before and after hot-air oven drying (FP 720, Binder GmbH, Tuttlingen, Germany) at 80 °C for 96 h. The DM content was then estimated as the ratio of dried to the fresh weight of the samples and expressed in percent (%).

2.2. Deep learning for pear fruit centroid detection

2.2.1. Image labelling for ground truth bounding boxes

The deep transfer learning, there was a need for supervised labelled spectral images for fining tuning the object detector. Hence, at first, for each image, the ground truth bounding box for each pear was manually labelled by selecting a rectangle enclosing the belly of the pear. The manual section was implemented using MATLAB (release R2021a, The MathWorks, Inc., Natick, MA, USA) built-in function *drawrectangle*.

2.2.2. Deep transfer learning

A pretrained YOLOv4 object detection network followed by transfer learning was employed for this task (Xu and Mishra, 2022). All programming was conducted in the MATLAB computing environment with the computing system of Intel(R) Core (TM) i7–6700 CPU@3.40 GHz processor. The application of deep transfer learning was based on the open-source scripts downloaded from: https://github.com/matlab-deep-learning/pretrained-yolo-v4. A detailed description regarding the network architecture can be found in earlier realted work (Xu and Mishra, 2022).

The objective of this work was to adapt the pre-trained YOLO v4 network to detect the pear fruit belly part. The training set consists of 1818 pears (from 111 images), while the test set has 72 pears (from 6 images), as exhibited in Table 1. The test set consisted of 6 images only as the 6 images belonged to the fruit stored at lower relative humidity conditions and can be considered as a new batch of data. Data augmentation including random horizontal flip, random scaling, and colour jitter augmentation in HSV space were also applied to increase the variety of training data. Random horizontal flip refers to the procedure of flipping the entire image horizontally. Random scaling was implemented by randomly changing the scale of the image. Colour jitter augmentation in HSV space was performed by randomly changing the brightness, contrast and saturation of the image. This work applied the Matlab built-in function *jitterColorHSV* to adjust the colour of RGB image with a randomly selected value of brightness, contrast and saturation from the HSV color space, with the range of each type of adjustment specified as 0.3, 0.4 and 0.2, respectively. The applied data augmentation methods allowed the generation of the artificial data to increase training data size, which was useful to improve the performance and outcomes of the deep learning model. The intial starting point for the model were the same pre-trained YOLOv4 weights as the earlier model (Xu and Mishra, 2022). The learning rate was set to 0.0001, batch size was 4, and the number of epochs was 90. The number of classes was set to 1, meaning that the model either detects the pear fruit belly or remains undetected.

To evaluate the model performance, a series of metrics that were obtained from the test set. First and utmost, the precision-recall curve allowed calculation of average precision (AP) that is defined as the averaged precision across all recall values between 0 and 1 at various Intersection over Union (IoU) ratio thresholds. AP represents the area under the curve of the precision-recall curve after interpolating across all points. The IoU ratio, which computes intersection over the union of the bounding box between the ground truth and the predicted bounding box, is also deemed important for model assessment. An IoU close to 1 shows the perfection prediction that the predicted bounding box has been perfectly overlapped with the ground truth.

2.3. Chemometric modelling for fruit property prediction

The chemometric modelling of the spectral data to predict DM was performed using the PLS modelling. The PLS modelling was chosen over the deep learning modelling as there was a low number of data points to train a deep spectral model. The model training was performed on the hydrated fruit samples (144 total) while the model independent testing was performed on the dehydrated fruit samples (72 total). The fruit were stored in two different air-tight 550 L controlled-flow storage containers (80 % N_2, 20 % O_2 and <0.7 % CO_2). The container lid was fitted in an empty water-lock for active dehydration treatments. For dehydration, 2.0 kg of silica gel (Merck KGaA, Darmstadt, Germany) was placed on the top of the container to generate two different dehydration environments for the pears. Silica gel was exchanged every 4 days for dried silica-gel to achieve dehydration. Pear fruit were stored under these conditions for 4 weeks and prior to spectral analysis were acclimated at 20 °C overnight. The fruit skin dehydration changes its physical structure (Mishra et al., 2022c). Since the spectral measurements were perfomed through the fruit skin it is expected that the dehydrated fruit had extra variation due to dehydrated skin which may challenge the PLS model based on hydrated fruit (Mishra et al., 2022a). The DM range for the training set was 13.52 ± 0.95 % and for the test set was 13.73 ± 1.01 %. Note that for PLS modelling, the spectra extracted from the centroid regions were used. For the test set, those centroids were first identified with the deep transfer learning based pear fruit belly detection as explained in an earlier section. Furthermore, in this study, the effect of the window width for extracting the mean spectral signal on PLS modelling was also explored. In total, 4 different spectral options for PLS calibration were explored i.e., the spectra correspond to centroid pixels, and the mean spectra obtained from three different windows of sizes (3, 7 and 11) surrounding the centroid pixel. Hence, in total, 4 PLS calibrations were performed to find the best option to extract the mean spectra for DM prediction in pear fruit. The best option was then used in combination with the object detecting to simultaneously detect the fruit belly and predict the DM in pear fruit. The PLS analysis was carried out using the data in the spectra range of 606–1000 nm as the data below 606 nm was noisier. The data were also pre-processed with the standard normal variate pre-processing (Barnes et al., 1989) to remove the additive and multiplicative effects usually disturbing the PLS modelling. The model performances were evaluated using the root mean squared error of prediction (RMSEP).

3. Results and discussion

3.1. Detection of pear fruit belly

An earlier study (Xu and Mishra, 2022) has shown the potential use of the YOLOv4 object detector for detecting multiple fruit types including apple, pear, black grape, green grape, blueberry, and kiwi. However, the model developed in earlier study is only suitbale when the fruit are symetterical. To visually show and compare the performance of the YOLOv4 object detector used in earlier work (Xu and Mishra, 2022)

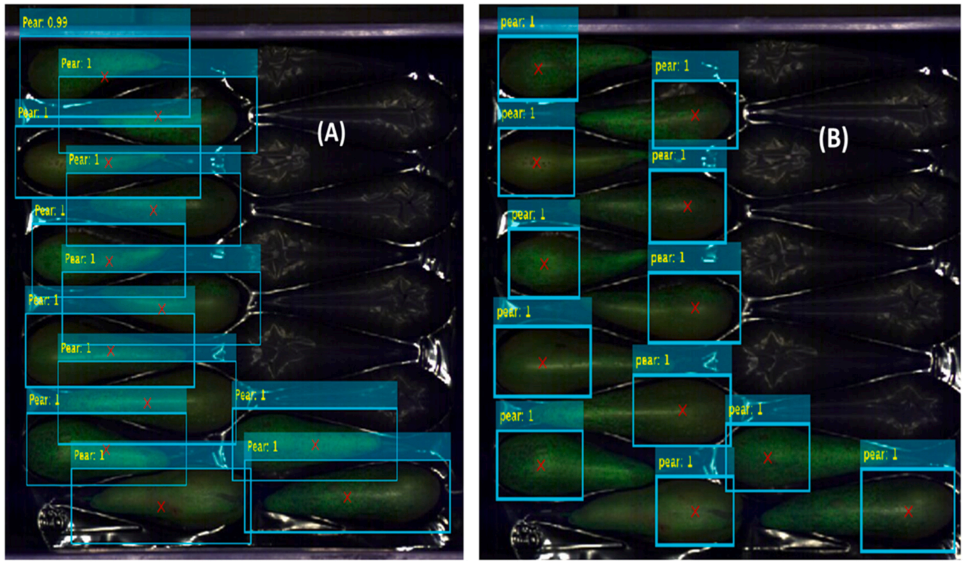

Fig. 2. : The detection results (bounding boxes, labels and probability scores) of applying YOLOv4 object detector from earlier work (Xu and Mishra, 2022) (A) and from this work aiming at the belly part of pears (B). The centroid pixel of each bounding box was indicated in the red cross.

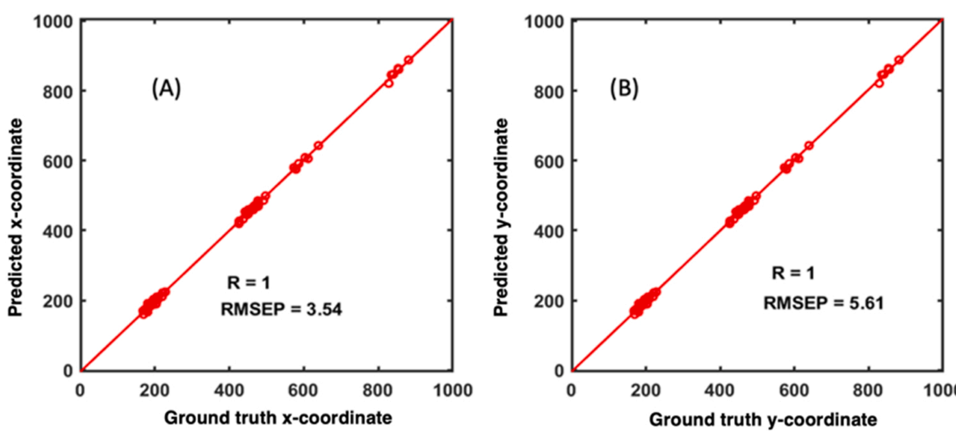

Fig. 3. Prediction plots for ground truth and predicted centroids. (A) x-coordinate of the centorids, and (B) y-coordinate of the centorids. The RMSEP unit is pixels.

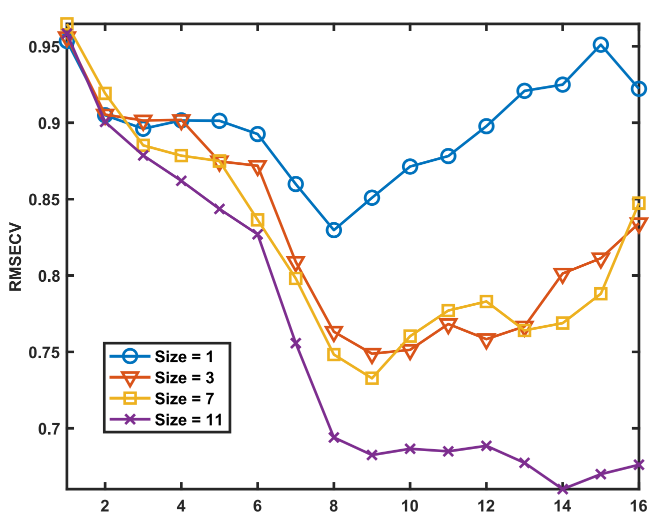

Fig. 4. 5-fold cross-validation analysis for PLS modelling performed on mean spectra extracted using different window widths. The size (pixels× pixels) explains the window width used to estimate the mean spectra for fruit.

and the fruit belly detection model from this work, the object detection maps are displayed in Fig. 2A and B, respectively. Notice that all the training and test images of this work were coming from the new batch that was not used in the earlier work. Fig. 2A demonstrated the performance in terms of recognizing and localizing all pear fruit with detection probability scores higher than 0.99, suggesting that the object detector from earlier work (Xu and Mishra, 2022) has good predictive ability encountering independent and unseen samples. Although the entire pear has been well identified, the centroid pixel (marked in a red cross) of each bounding box is not located on the wanted belly part due to the asymmetrical nature of pear fruit, which brings up the need for this work. In Fig. 2B, it can be seen that the current object detector is capable of localizing the belly part of the pear, providing the satisfying centroid pixel which can be used for chemometric predictive modelling. Additionally, high probability scores (>0.99) were also witnessed. The performance metrics of applying the pre-trained YOLOv4 object detector combined with transfer learning to detector the belly area of pears are shown in Table 1. The precision-recall curve is not presented because precision values were always equal to 1 at various thresholds, showing that the model performed well. The strong prediction capability for the detection of the belly part of the pear was also confirmed with the AP of 1. Fig. 3 presents the predicted bounding versus ground truth centroid pixels. Optimal matching (with a correlation coefficient of 1) between

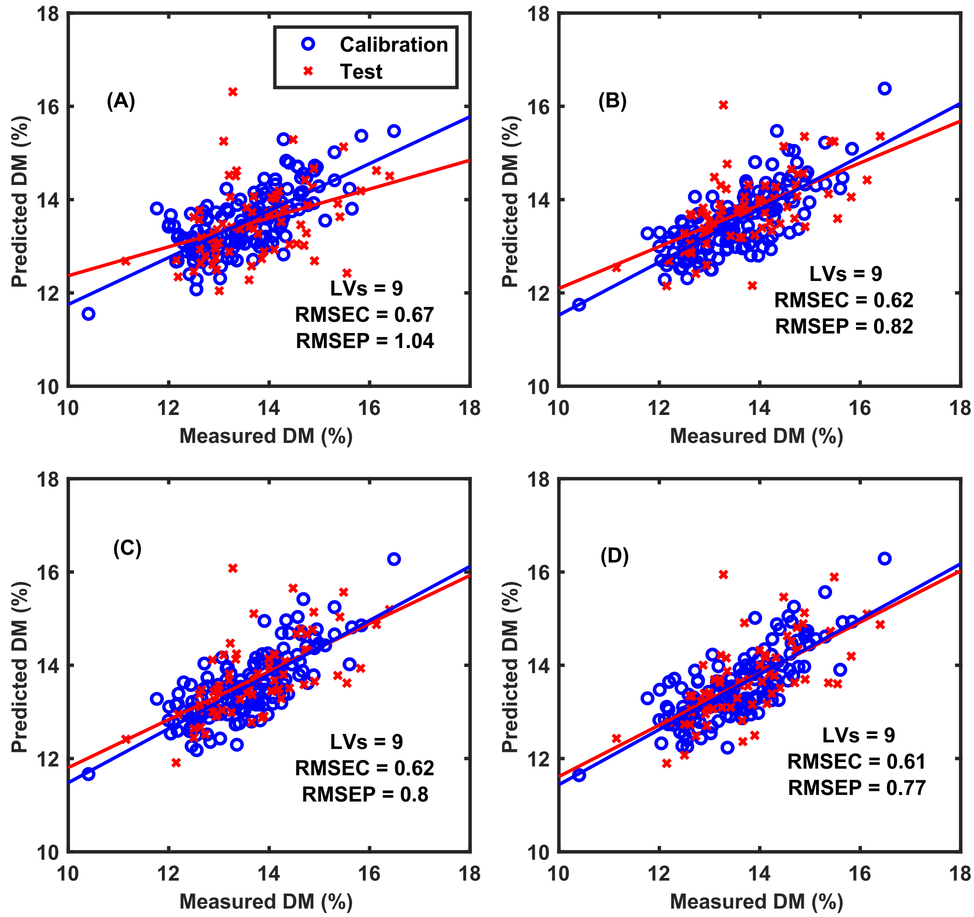

Fig. 5. Prediction plots for PLS models calibration using mean spectra extracted using different window widths. (A) Centroid pixels, (B) mean spectra extracted with window width of 3, (C) mean spectra extracted with window width of 7, and (D) mean spectra extracted with window width of 11.

predicted and actual centroids was noted, consistent with the high value of mean IoU (0.82). Note that the IoU scores was not 1 due to the fact that for some samples the human labelling was not perfect compared to the detection by the deep learning model. The average processing time calculated from running 100 times of applying the object detector on one image of the test set was found to be 0.46 s. Dividing by 12 pear objects, results implied that deploying the current object detection model to localize the belly area of each pear requires the processing time of 0.038 s, having the potential to fulfil the requirement for real-time applications.

3.2. Chemometric model application on the centroid of fruit belly

In earlier study (Xu and Mishra, 2022), it was found that the selection of the window width for estimating the mean spectral responses from the object can have a big influence on the chemometric model performance. For example, choosing a low window width can lead to poor performance than the large window width. In this study, the effect of changing the window width on the PLS model calibration and the test was explored. The results of cross-validation analysis based on mean spectra extracted using different window width sizes are shown in Fig. 4. It can be noted that as the window width increases the cross-validation error become lower, indicating that the choice of using the single centroid pixel for chemometric modelling was the worst. The results were further confirmed when the models were calibrated and tested using the same number of latent variables = 9. The prediction error (RMSEP) was lower for the PLS analysis carried out using the mean spectra extracted with a window width of 11 compared to the PLS analysis based on a single centroid pixel. Such lower prediction error led to the choice of the window width = 11 as the optimal for the final model application. The trend of the RMSECV (Fig. 4) and RMSEP (Fig. 5), indicates that increasing the window width beyond 11 can further reduce the errors, however, increasing the window size beyond 11 can make the window width greater than the fruit and end up including the non-fruit pixels for the average which can naturally deteriorate the model performance. The RMSEP = 0.77% is what is usually noted with the NIR technique for pear fruit analysis (Mishra et al., 2021a; Mishra and Woltering, 2021; Mishra et al., 2021b; Travers et al., 2014).

Due to the advances in computer vision, the application of deep learning models for the task of fruit detection and localisation has been reported over recent years (Koirala et al., 2019). A recent study (Parico and Ahamed, 2021) was published to develop a real-time pear fruit counter for mobile applications using YOLOv4 models, producing the optimal average precision of 0.98. This work generates a higher AP partly because of a simpler indoor background in our case compared to the reported study (Parico and Ahamed, 2021) that was performed in the orchard. It is also worth pointing out that most reported studies attempted to detect the entire fruit, yet in our case, we innovatively apply a deep learning model to detect the area of interest from the fruit.

In many scientific works related to hyperspectral imaging of fruit (Lu et al., 2020), the experiments are performed with customised imaging setups. This is because currently, the spectral cameras are readily available but always require system integration before their use. Different scientific practitioners usually end up developing their spectral imaging systems which may influence the repeatability of the hyperspectral imaging technology. In that regard, the ASI system (Fig. 1) for hyperspectral imaging allows to perform standardised spectral imaging measurements on fruit samples as all the hardware and image acquisition settings are fixed. The emergence of deep learning approaches for hyperspectral image processing for fresh fruit is also a new topic. In some earlier studies deep learning based approaches such as stacked autoencoders were used (Yu et al., 2018b,a), however, those studies mainly used deep learning to perform predictive modelling to replace PLS based analysis. However, in some recent studies, it has been shown that for spectral data modelling PLS approach is more generalised compared to the current state-of-the-art deep learning approaches such as one-dimensional convolutional neural networks (Mishra and Passos, 2021) and stacked autoencoders (Mishra et al., 2021c). This was also the motivation that this study only used deep learning for object detection and not for predictive modelling. The predictive modelling was carried out using the PLS analysis.

One of the main motivations behind the use of hyperspectral imaging for fruit analysis is its capability to provide the spatial distribution of properties in fruit (Lu et al., 2020). However, in the current work, the aim was not to explore the spatial properties but was high-throughput prediction of average DM content in pears. For example, in the current ASI system (Fig. 1), a crate full of fruit can be analysed for DM with a single scan. In any case, if the interest is to predict spatial distribution then instead of estimating the average DM, the prediction can be made pixel-wise leading to prediction maps. Nevertheless, the acquisition, storing and processing of hyperspectral images covering a big scene is inevitably time-consuming and computationally expensive. In this regard, this work has opened new possibilities for real-time applications by taking full advantage of DL and chemometrics. For a real-time application scenario, an extended RGB image is first collected, based on which the area of interest of individual fruit objects can be successfully detected and localized using YOLOv4 object detector. The relevant spectral image or spectroscopy only needs to be collected from these areas of interest to predict the chemical properties, which will remarkably speed up the entire pipeline of analysis.

4. Conclusions

A novel case of combining deep learning and chemometric modelling to process spectral images was demonstrated. Particularly, the study involved detection of symmetrical part in asymmetrical objects to locate the object centroid. In the presented case of pear fruit analysis, the deep transfer learning using 111 spectral images allowed to train a high precision (100 %) fruit belly detection model which simplified the development and application of the PLS predictive model. It was also found that the choice of the window width for extracting the mean spectra of fruit can have a big influence on the PLS model learning and predictive performance. In the presented case, a window width of 11 (extracting 121 pixels) was found to be delivering the lowest prediction errors RMSEP = 0.77 %. Furthermore, both the object detector combined with the PLS predictive model provided a practical approach to spectral image processing where the deep learning was able to deal with the image processing challenges and the PLS modelling allowed dealing with the spectral modelling. The presented approach can have wide implications for automating spectral image processing, particularly when real practical applications of spectral imaging need to be developed.

CRediT authorship contribution statement

Junli Xu: Conceptualization, Methodology, Software, Formal analysis, Writing - Original Draft **Puneet Mishra**: Conceptualization, Methodology, Software, Formal analysis, Writing - Original Draft.

Declaration of Competing Interest

The authors declare that they have no known competing financial interests or personal relationships that could have appeared to influence the work reported in this paper.

Acknowledgements

Puneet Mishra acknowledges that a part of data used in this study for training deep learning model was generated during the LNV (Dutch Ministry of Agriculture, Nature and Food Quality, The Netherlands) funded Sensing Potential project (ref: KB-38–001-008).

References

Anderson, N.T., Walsh, K.B., Subedi, P.P., Hayes, C.H., 2020. Achieving robustness across season, location and cultivar for a NIRS model for intact mango fruit dry matter content. Postharvest Biol. Technol. 168 (111202).
Barnes, R.J., Dhanoa, M.S., Lister, S.J., 1989. Standard normal variate transformation and de-trending of near-infrared diffuse reflectance spectra. Appl. Spectrosc. 43 (5), 772–777.
Koirala, A., Walsh, K.B., Wang, Z., McCarthy, C., 2019. Deep learning – method overview and review of use for fruit detection and yield estimation. Comput. Electron. Agric. 162 (219–234).
Lammertyn, J., Peirs, A., De Baerdemaeker, J., Nicolaï, B., 2000. Light penetration properties of NIR radiation in fruit with respect to non-destructive quality assessment. Postharvest Biol. Technol. 18 (2), 121–132.
Lin, X., Xu, J.-L., Sun, D.-W., 2021. Comparison of moisture uniformity between microwave-vacuum and hot-air dried ginger slices using hyperspectral information combined with semivariogram. Dry. Technol. 39 (8), 1044–1058.
Lu, Y., Saeys, W., Kim, M., Peng, Y., Lu, R., 2020. Hyperspectral imaging technology for quality and safety evaluation of horticultural products: A review and celebration of the past 20-year progress. Postharvest Biol. Technol. 170 (111318).
Mahlein, A.K., Kuska, M.T., Behmann, J., Polder, G., Walter, A., 2018. Hyperspectral sensors and imaging technologies in phytopathology: state of the art. Annu. Rev. Phytopathol. 56 (1), 535–558.
Mishra, P., 2021. Deep generative neural networks for spectral image processing. Anal. Chim. Acta 1191, 339308.
Mishra, P., Passos, D., 2021. Deep chemometrics: Validation and transfer of a global deep near-infrared fruit model to use it on a new portable instrument. J. Chemom. 35 (10), e3367.
Mishra, P., Woltering, E., 2021. Handling batch-to-batch variability in portable spectroscopy of fresh fruit with minimal parameter adjustment. Anal. Chim. Acta 1177 (338771).
Mishra, P., Lohumi, S., Ahmad Khan, H., Nordon, A., 2020. Close-range hyperspectral imaging of whole plants for digital phenotyping: Recent applications and illumination correction approaches. Comput. Electron. Agric. 178 (105780).
Mishra, P., Roger, J.-M., Rutledge, D.N., 2021. A short note on achieving similar performance to deep learning with practical chemometrics. Chemom. Intell. Lab. Syst. 214 (104336).
Mishra, P., Marini, F., Brouwer, B., Roger, J.M., Biancolillo, A., Woltering, E., Echtelt, E., H.-v, 2021a. Sequential fusion of information from two portable spectrometers for improved prediction of moisture and soluble solids content in pear fruit. Talanta 223 (121733).
Mishra, P., Woltering, E., Brouwer, B., Hogeveen-van Echtelt, E., 2021b. Improving moisture and soluble solids content prediction in pear fruit using near-infrared spectroscopy with variable selection and model updating approach. Postharvest Biol. Technol. 171 (111348).
Mishra, P., Brouwer, B., Meesters, L., 2022. Improved understanding and prediction of pear fruit firmness with variation partitioning and sequential multi-block modelling. Chemom. Intell. Lab. Syst. 222 (104517).
Mishra, P., Paillart, M., Meesters, L., Woltering, E., Chauhan, A., 2022a. Avocado dehydration negatively affects the performance of visible and near-infrared spectroscopy models for dry matter prediction. Postharvest Biol. Technol. 183 (111739).
Mishra, P., Sytsma, M., Chauhan, A., Polder, G., Pekkeriet, E., 2022b. All-in-one: A spectral imaging laboratory system for standardised automated image acquisition and real-time spectral model deployment. Anal. Chim. Acta 1190 (339235).
Parico, A.I.B., Ahamed, T., 2021. Real time pear fruit detection and counting using YOLOv4 models and deep SORT'. Sensors 21 (14), 4803.
Rungpichayapichet, P., Nagle, M., Yuwanbun, P., Khuwijitjaru, P., Mahayothee, B., Müller, J., 2017. Prediction mapping of physicochemical properties in mango by hyperspectral imaging. Biosyst. Eng. 159 (109–120).
Subedi, P.P., Walsh, K.B., 2020. Assessment of avocado fruit dry matter content using portable near infrared spectroscopy: Method and instrumentation optimisation. Postharvest Biol. Technol. 161.
Travers, S., Bertelsen, M.G., Petersen, K.K., Kucheryavskiy, S.V., 2014. Predicting pear (cv. Clara Frijs) dry matter and soluble solids content with near infrared spectroscopy. Lwt-Food Sci. Technol. 59 (2), 1107–1113.
Walsh, K.B., Blasco, J., Zude-Sasse, M., Sun, X., 2020. Visible-NIR 'point' spectroscopy in postharvest fruit and vegetable assessment: the science behind three decades of commercial use. Postharvest Biol. Technol. 168 (111246).

Xu, J., Mishra, P., 2022. Combining deep learning with chemometrics when it is really needed: a case of real time object detection and spectral model application for spectral image processing. Anal. Chim. Acta 339668.
Yu, X., Lu, H., Liu, Q., 2018. Deep-learning-based regression model and hyperspectral imaging for rapid detection of nitrogen concentration in oilseed rape (Brassica napus L.) leaf. Chemom. Intell. Lab. Syst. 172 (188–193).
Yu, X.J., Lu, H.D., Wu, D., 2018. Development of deep learning method for predicting firmness and soluble solid content of postharvest Korla fragrant pear using Vis/NIR hyperspectral reflectance imaging. Postharvest Biol. Technol. 141 (39–49).